Microstructure and Mechanical Properties of Reticulated Titanium Scrolls**

By *Eunji Hong, Bok Y. Ahn, Daisuke Shoji, Jennifer A. Lewis* and *David C. Dunand**

Reticulated titanium scrolls are produced by printing titanium hydride lattices composed of two orthogonal layers of ink filaments, which are then rolled into cylinders and reduced to titanium upon partial vacuum sintering. The resulting three-dimensional titanium scrolls contain a hierarchical pore size distribution composed of macroporosity between patterned filaments and micropores within each filament. These reticulated architectures exhibit an attractive combination of stiffness, strength, and ductility when tested in uniaxial compression.

[*] Prof. D. C. Dunand
Department of Materials Science and Engineering,
Northwestern University,
Evanston, IL 60208, (USA)
E-mail: dunand@northwestern.edu
E. Hong
School of Advanced Materials Engineering,
Kookmin University,
861-1 Jeongneung-dong, Seongbuk-gu,
Seoul 136-702, (Republic of Korea)
Previously with Department of Materials Science and
Engineering, Northwestern University, Evanston, IL 60208, (USA)
Dr. B. Y. Ahn, Prof. J. A. Lewis
Department of Materials Science and Engineering, University
of Illinois at Urbana-Champaign, Urbana, IL 61801, (USA)
D. Shoji
Pentax New Ceramics Division,
Hoya Corporation, Tokyo 174-8639, (Japan)
Previously with Department of Materials Science and
Engineering, University of Illinois at Urbana-Champaign,
Urbana, IL 61801, (USA)

Titanium and its alloys find widespread use in skeletal implants and biomedical devices (e.g., stents and orthodontic applications) owing to their excellent corrosion resistance, bio-compatibility, static and fatigue strength, and lack of magnetism (an important property for magnetic imaging).[1] Microporous titanium provides two additional advantages for implant applications: first, it reduces the stiffness of the material, thus reducing stress shielding,[2,3] and, second, it improves implant anchorage by allowing bone ingrowth.[4–6] To date, powder metallurgy approaches have been widely used to create porous Ti structures, through partial sinter-ing,[7–9] inclusion of pore formers,[10–13] expansion of pores pressurized with argon or hydrogen gas,[14,15] or replication of cellular polymers.[16,17] Embrittlement often arises during processing due to the strong chemical affinity of titanium at elevated temperature with atmospheric oxygen, carbon, and nitrogen. Alternate efforts have focused on producing microarchitectured titanium, composed of lattice or truss structures with struts arranged periodically in space. These structures exhibit an outstanding combination of low density, high strength and stiffness, and good damage tolerance.[18] To date, production methods for microarchitectured titanium have focused on replication precision casting,[19,20] sintering of stacked wire arrays,[21] as well as selective electron beam,[22–24] or laser[25] sintering of Ti powders.

Recently, we introduced a new method for creating 3D microarchitectured Ti structures that combines:[26] (i) direct ink writing (DIW) of planar lattices composed of two layers of orthogonally oriented, patterned TiH_2 filament arrays, followed by (ii) rolling of these pliable lattices into scrolls, or folding into complex three-dimensional shapes, and finally (iii) heat-treating to reduce the hydride to metallic titanium. This new method is characterized by its simplicity, high shape versatility, and ability to control local geometry, as well as scalability to larger structures.[26] Here, we use this novel

approach to produce reticulated Ti scrolls and characterize their microstructural and mechanical properties upon vacuum sintering.

Experimental

We formulated two types of TiH$_2$-based inks for direct-write assembly. The first ink consists of titanium hydride powder (TiH$_2$, 4.4 wt% H$_2$, Alfa Aesar, MA, USA), a triblock copolymer composed of poly(methyl methacrylate)-poly(*n*-butylacrylate)-poly-(methyl methacrylate) (PMMA-P*n*BA-PMMA, molecular weight of 23 000–31 000–23 000 g · mol^{-1}, Kuraray Co., Ltd., TX, USA), and a graded-volatility solvent mixture of dichloromethane (b.p. 40 °C), 2-butoxyethanol (b.p. 171 °C), and dibutyl phthalate (b.p. 340 °C) (Fig. 1b). The TiH$_2$ particle size distribution ranges from 0.5 to 90 μm, with a mean particle size of 22 μm. The ink is prepared by first dispersing 9 g TiH$_2$ powder in 4 g dichloromethane, 1.2 g 2-butoxyethanol, and 0.6 g dibutyl phthalate by sonication (FS30, Fisher Scientific, PA, USA) for 30 min at room temperature. Next, 7.2 g of triblock copolymer solution (20 wt% in dichloromethane) is added to the resultant suspension to yield a copolymer:TiH$_2$ ratio of 1:6 by weight. This suspension is sonicated for 10 min, and then concentrated by solvent evaporation to yield an ink with a total solids loading of ≈85 wt% (≈73 wt% TiH$_2$ and ≈12 wt% copolymer).[26] This ink, referred to the TiH$_2$ (22 μm) ink, readily flows through deposition nozzles with diameters of 200 − 500 μm, is stable for several months when properly sealed, and is readily re-dispersed in organic solvents (e.g., toluene and ether) to form a less viscous ink. A second ink, composed of TiH$_2$ with a narrower particle size distribution (40 − 90 μm) and a larger mean size of 65 μm, is obtained by sieving the above 0.5 − 90 μm TiH$_2$ powder with a 40 μm sieve. This ink, hereafter, referred to as the TiH$_2$ (65 μm) ink, contained 73 wt% TiH$_2$ powder with a copolymer:TiH$_2$ ratio of 1:6 by weight.

As a control, a nanoparticle titanium ink is also formulated, hereafter, referred to as the Ti (0.1 μm) ink, which contains 79 wt% Ti powder (Sigma–Aldrich, MO, USA) with a mean particle size below 0.1 μm, at a copolymer:Ti ratio of 1:12 by weight. The dramatically reduced particle size is expected to enhance sintering. Because TiH$_2$ powders are not available in sub-micrometer size, metallic Ti powders are used in this ink, despite their very high reactivity leading to contamination during heat treatment.[27] The as-received Ti nanoparticles are dispersed in mineral oil and washed in dichloromethane before ink formulation. The copolymer content is optimized for each ink to ensure its flow through a 250 μm diameter nozzle as well as its ability to form spanning features. For example, the copolymer:metal ratio of 1:12 ratio is suitable for the Ti (0.1 μm) ink, but the same copolymer content results in nozzle clogging for the TiH$_2$ (65 μm) ink due to its higher stiffness.

The ink meshes are produced using a three-axis micro-positioning stage (ABL 9000 *x*–*y*–*z* motion stage, Aerotech Inc., PA, USA), whose motion is controlled by computer-aided design software (RoboCAD, OK, USA) under ambient conditions. The concentrated ink is transferred into a syringe (Fig. 1b) and extruded through a 250 μm diameter nozzle (Fig. 1a) on a glass substrate to create rectangular meshes (25 × 10 × 0.4 mm^3) consisting of two orthogonal layers of ink filament (240 ± 20 μm diameter) arrays with a 700 μm center-to-center spacing between filaments. After drying for 10 min under ambient conditions, the printed lattices are rolled using a custom-designed apparatus into ''scrolls'' (Fig. 1c), as opposed to high aspect ratio ''towers'' formed solely by printing.[28,29] As described in ref.[26] the solvent must be partially evaporated to a point where the printed lattice is pliable, with ink filaments neither sagging due to excess solvent nor cracking due to too little solvent. After the appropriate solvent loss is achieved, the printed structures are flexible enough to manipulate and bend, but firm enough to retain their shape after rolling. The scroll height and diameter are determined by the dimensions of the printed lattices.

The fabricated scrolls are heat-treated in a high-vacuum furnace with $10^{-5} − 10^{-6}$ torr residual pressure. The procedure involves three separate stages: (i) a debinding stage consisting of three 2 h-holds at 200, 250, and 300 °C to remove the triblock copolymer; (ii) a dehydriding stage at 600 °C for 2 h to decompose the hydride into metallic titanium [this stage is not necessary for the Ti (0.1 μm) ink]; and (iii) a sintering stage at 1 050 °C for 10 h to sinter the titanium powder. The heating rate for stages (i), (ii), and (iii) is 2, 5, and 7 °C · min^{-1}, respectively, with all scrolls furnace-cooled under vacuum.

Before and after heat-treatment, the scrolls are weighed and their diameter and height are measured with vernier calliper and a micrometer at >10 locations to quantify changes in their diameter and calculate their total porosity. Some titanium scrolls are cut with a diamond saw, mounted, and polished following standard metallographic procedures. Optical microscopy and SEM are used to examine the Ti scrolls and their cross-sections on which hardness is determined using a Vickers microhardness tester (Struers, OH, USA). Uniaxial compressive tests are performed on two
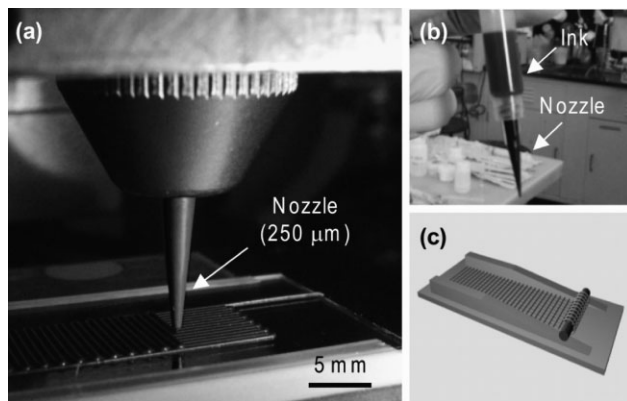

Fig. 1. (a) Optical image acquired during direct writing of the TiH$_2$ (22 μm) ink (≈ 85 wt% solids) on a glass substrate. (b) Optical image of an ink-filled syringe barrel (3 ml) with a 250 μm diameter tapered nozzle. (c) Schematic illustrating the custom-designed rolling apparatus, using a solid core.

titanium scrolls with flat and parallel polished end surfaces, a diameter of 2.8 mm, and a height-to-diameter ratio of $1.5 - 2$, using a Sintech 20/G testing apparatus (MTS System Corporation, NC, USA) at a nominal strain rate of $0.001\,s^{-1}$ with a 8 KN load cell. Strain is determined from crosshead displacement, after subtracting machine compliance using calibration loading curves on aluminum samples.

Results and Discussion

Printed and Rolled TiH₂ Scrolls

Figure 2a and b shows SEM micrographs of printed lattices produced using the TiH_2 (22 µm) ink. The TiH_2 particles are closely packed and the overall cylindrical shape of each printed filament (230 ± 10 µm) is maintained. The filament size can be varied by adjusting nozzle diameter, printing speed, or applied pressure. Figure 2c shows a SEM micrograph of a dried TiH_2 mesh with a center-to-center filament spacing of 0.7 mm, which is defined by the computer program that controls the printing stage. Neither sagging nor deformation of ink filaments within the printed lattices is observed. Figure 2d shows an optical image of three scrolls rolled from printed TiH_2 lattices ($12 \times 30 \times 0.4$ mm³, filament

diameter ≈ 250 µm, center-to-center filament spacing of 0.7 mm), in which rolling is carried out with or without a central titanium tube (inside and outside diameters of 1.0 and 1.5 mm), and a rod with 2.0 mm diameter. As demonstrated in ref.[26], many shape variations are possible, including spirally coiled helices, stents, and hollow cylindrical structures that can be produced by rolling meshes onto support structures that are removed prior to drying and sintering.

Microstructure and Hardness of Annealed Ti Scrolls

Figure 3a and b shows SEM micrographs of a representative scroll created from the TiH_2 (22 µm) ink before and after sintering, taken as edge, side, and top views, respectively. It is apparent that neither collapse nor distortion occurs during heat treatment, despite the large volumetric shrinkage of $41 \pm 1\%$ observed, which corresponds to a 15 ± 1 and a $19 \pm 0\%$ reduction in diameter and height, respectively. The reported values represent the average values and standard deviations for a set of two TiH_2 (22 µm) ink scrolls.

Figure 4a–f shows optical micrographs of mounted and polished cross-sections of titanium scrolls printed from the two TiH_2 (65 and 22 µm) inks and the Ti (0.1 µm) ink. In all cases, orthogonal filaments within the flat double-layered titanium mesh are well bonded with clearly defined sintering necks (arrows 1 in Fig. 4f); bonding of filaments across meshes is less extensive (arrow 2 in Fig. 4f) and in some cases even nonexistent (arrow 3 in Fig. 4f). Micropores (with size under $\sim$30 µm) are present in the filaments of all scrolls, with their volume fraction decreasing as the particle size decreases (Fig. 4b, d, and f), as expected from their improved sinterability.
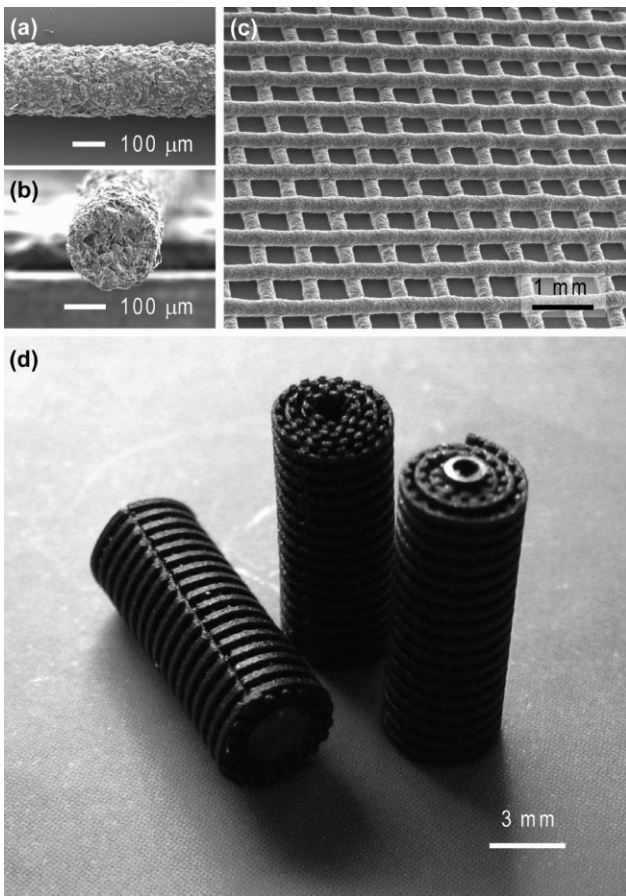

Fig. 2. SEM micrographs of printed TiH₂ (22 µm) filaments (a) top view and (b) cross-sectional view. (c) SEM micrograph of printed lattice using the TiH₂ (22 µm) ink. (d) Photograph of TiH₂ scrolls, fabricated by rolling a printed lattice onto a titanium rod (left), with the rod removed (middle), and onto a titanium tube (right).
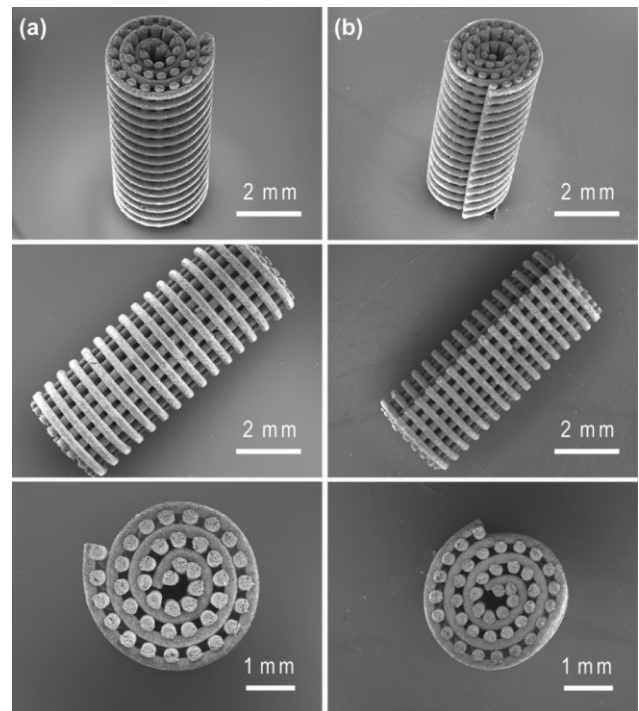

Fig. 3. SEM micrographs of edge, side, and top views before (a, left column) and after annealing (b, right column) of the same scroll created with the TiH₂ (22 µm) ink.
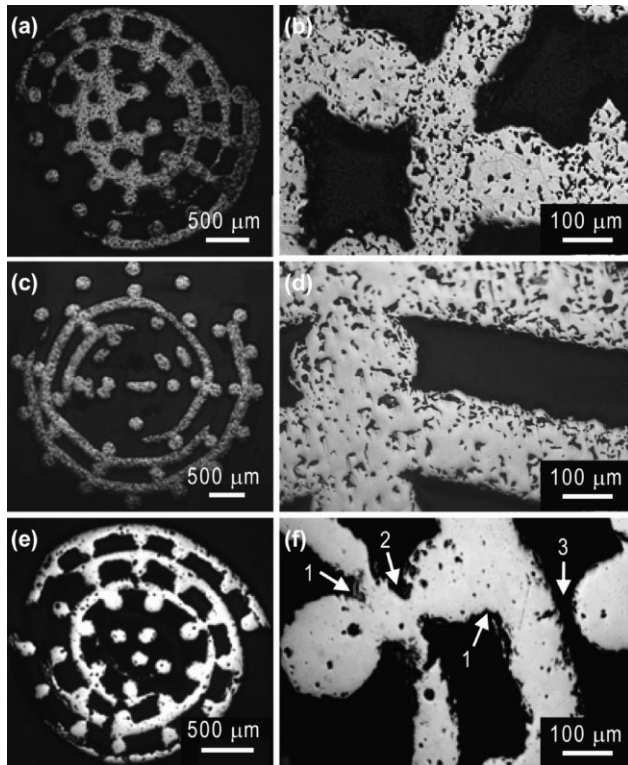
Fig. 4. Optical micrographs of polished cross-sections of heat-treated titanium scrolls created with (a and b) TiH₂ (65 μm) ink, (c and d) TiH₂ (22 μm) ink, (e and f) Ti (0.1 μm) ink. Sintering necks (marked with 1 and 2) connect filaments but are sometime missing (3).

Mean filament diameter and spacing obtained from optical images of titanium scrolls printed from the TiH_2 (22 μm) ink are 180 ± 13 μm and $135 - 175$ μm, respectively. The cross-sectional area of these filaments decreased by $39 \pm 8\%$, consistent with an overall volume change of $41 \pm 1\%$. Residual micropores have been observed in other powder-metallurgy studies on closed-porosity titanium foams created from TiH_2 formulations via a gel casting process[27] or a method using organic pore formers,[30] where microporosity decreased with decreasing polymer content.[30] The presence of micropores decreases the strength and stiffness of the struts aligned with the applied load, thus weakening the scrolls, and making them more compliant. This latter effect may be desirable for bone implants to prevent stress shielding, as previously discussed.

Vickers hardness of the scrolls produced with the TiH_2 ink (298 ± 50 HV for 22 μm ink and 310 ± 40 HV for 65 μm ink) corresponds to an oxygen content of ≈ 0.55 wt% O.[31] By contrast, the hardness of scrolls made with the Ti (0.1 μm) ink (809 ± 30 HV) is approximately three times higher, indicating extraordinarily high oxygen content. This hardness trend is consistent with the increased oxygen contamination expected due to the significantly higher surface area of the Ti nanoparticles as well as titanium's enhanced intrinsic reactivity relative to TiH_2, since oxygen is a potent strengthener and embrittler in titanium.[32]

Compressive Behavior of Ti Scrolls

Compressive tests are carried out solely on titanium scrolls created with the TiH_2 (65 μm) ink, whose struts displayed hardness (and thus strength and ductility) close to commercial
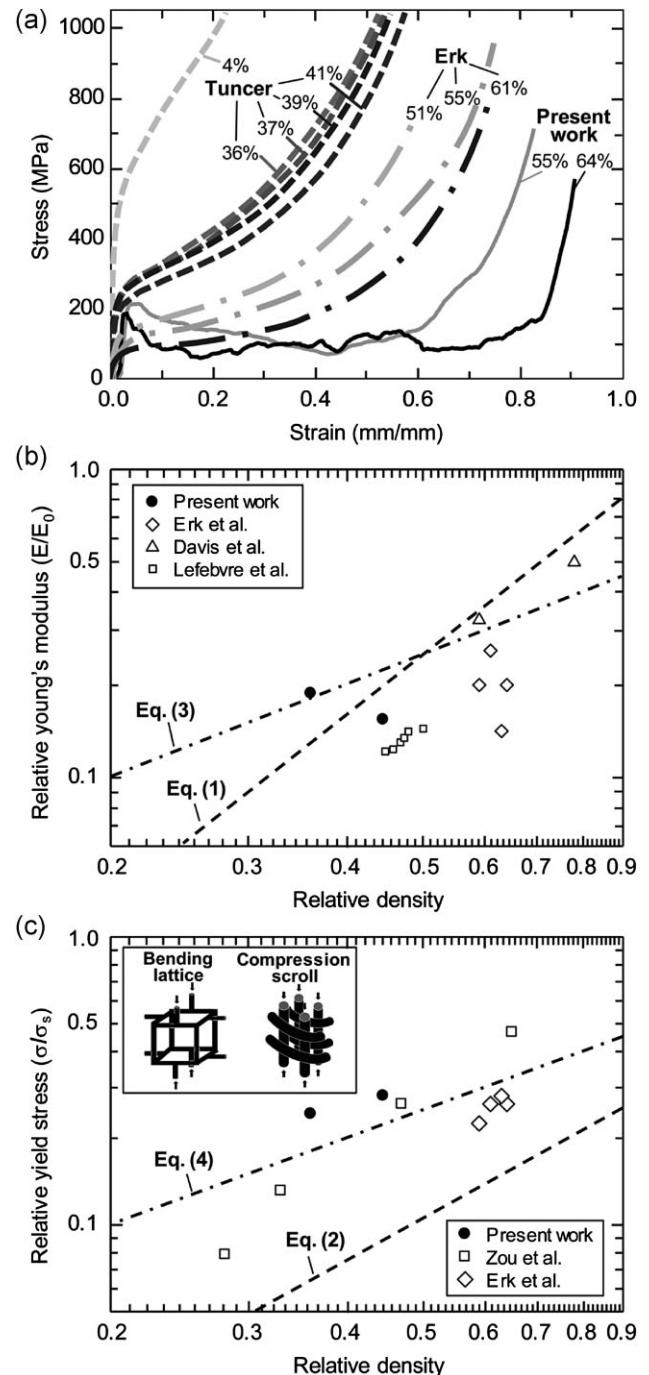

Fig. 5. (a) Compressive strain–stress curves for two titanium scrolls (estimated 0.55 wt% O) with 55 and 64% porosity created with TiH₂ (65 μm) ink, compared to titanium foams with 36 − 41% equiaxed pores (0.60 − 0.71 wt% O)[27] and 51 − 61% equiaxed pores (0.40 wt% O).[33] Plots of (b) Young's modulus and (c) yield stress (both normalized to the Young's modulus and yield strength of bulk titanium, respectively), versus relative density of the two titanium scrolls shown in figure (created with the TiH₂ (65 μm) ink). For comparison, data for other Ti foams are also plotted.[27,35–37] Solid yield strengths are σₛ = 735 MPa for the present scrolls (estimated, see text), and 760 MPa for Erk et al.[27] (measured) and for Zou et al.[35] (assumed, no measurement reported).

titanium. Figure 5a shows stress–strain curves for titanium scrolls with 55 and 64% porosity, which exhibit the three distinct regions typical of porous metals: (i) linear elasticity at low strains, (ii) a long plastic plateau punctuated by numerous small stress drops at higher strains, and (iii) a densification regime with steeply rising stresses. Neither scroll showed spalling or splitting, up to the end of region (iii) where the engineering strain reached 80–90%. The transition between regions (i) and (ii) is characterized by a peak stress beyond which the stress plateau shows a steady decrease in stress (to half the peak value) occurring over a 15–30% strain, followed by a regime of mostly constant stress, until densification occurs. By contrast, different behavior is observed for closed-cell titanium foams with equiaxed pores,[27] which show no peak stress, but whose plateau region (ii) is much shorter, smoother, and characterized by a slow increase in stress to region (iii), and are thus less capable of absorbing energy at low stresses (Fig. 5a). Serrations are visible in the stress–strain curves of the scrolls, which likely arise due to strut fracture, followed by crack propagation, either in the weaker bonds between struts (arrows 1 and 2 in Fig. 4f) or within them.

The Young's modulus of an open-cell foam E^* can be obtained from the linear elastic region of its strain–stress curve, and is predicted as a function of its relative density ρ using the Gibson and Ashby model:[34]

$$\frac{E^*}{E_s} = C_1 \left(\frac{\rho}{\rho_s}\right)^2 \tag{1}$$

where C_1 is a constant equal to unity, and E_s and ρ_s are the Young's modulus and density of the bulk metal, taking values of $E_s = 120\,GPa$ and $\rho_s = 4.51\,g \cdot cm^{-3}$ for titanium.[31] Similarly, the yield strength σ^* of open-cell metallic foams can be predicted by the Gibson and Ashby[34] model, assuming deformation by plastic hinging at the strut joints:

$$\frac{\sigma^*}{\sigma_s} = C_2 \left(\frac{\rho}{\rho_s}\right)^{3/2} \tag{2}$$

where C_2 is a constant equal to ≈ 0.3, and σ_s is the yield strengths of bulk titanium. For the titanium scrolls, we estimate a value σ_s of 735 MPa, which corresponds to CP-Ti with a hardness of 300 HV and an oxygen content of 0.55 wt%.[31] The normalized Young's modulus and compressive yield strength of the two scrolls are also plotted as a function of the relative density in a double logarithmic scale in Figure 5b and c, and compared with the predictions of Equations (1 and 2), respectively.

The Ti scrolls exhibit stiffness values that are in reasonable agreement with Young's modulus predictions from Eq. (1), given the large experimental errors associated with stiffness measurements during compressive deformation, sample settling, parallelism and early onset of plasticity at stress concentrations. Interestingly, however, the scrolls show much higher strengths than predicted by Equation (2). This observation is likely due to the fact that this equation is based on bending of struts, corresponding to a much weaker geometry than that present in the scrolls. The scroll architecture can be described as vertical struts, acting as compressive columns, connected to horizontal struts, preventing the buckling of the vertical columns (both architectures are shown schematically in the inset of Fig. 5c). A simplified model assumes that the vertical struts are in pure compression, with the horizontal strut carrying no load (but preventing buckling). For this case, the equations for stiffness and yield strength are:[21,38]

$$\frac{E^*}{E_s} = C_3 \left(\frac{\rho}{\rho_s}\right) \tag{3}$$

$$\frac{\sigma^*}{\sigma_s} = C_3 \left(\frac{\rho}{\rho_s}\right) \tag{4}$$

where $C_3 = {}^1/_2$ is the volumetric ratio of vertical to total struts. The stiffness of sample 1 is now in good agreement with prediction of Equation (3), while that for sample 2 seems too low (since it is lower than that of the less dense sample 1). The strengths calculated from Equation (4) are significantly higher than those determined from Equation (2), but remain $\approx 25\%$ below the measured values. This discrepancy may be due to inaccuracies in the estimate of σ_s of 735 MPa for bulk titanium (based on hardness, as discussed above) and to some load-bearing capacity from the horizontal struts. This hypothesis can be examined by finite-element modeling, which also allows consideration of the microporosity in the struts and the detailed geometry of the bond between struts (arrows 1 and 2 in Fig. 4f).

Generalization of Process

The novel DIW/rolling/sintering process developed for titanium is applicable to other metals (and alloys) which fall in four main categories: (i) noble metals (e.g., Ag, Au, Pt, and Pd) for which fine powders do not oxidize during the wet process and can be sintered without reduction; (ii) oxidation-resistant metal powders (e.g., Ni and stainless steel), which show only a thin oxide layer in powder form that does not prevent sintering; (iii) metals whose oxides can be reduced by hydrogen during sintering (e.g., Fe, Ni, Co, and Cu); and (iv) metals whose compounds can be decomposed during sintering (e.g., ZrH_2 and TiH_2, to create Zr and Ti scrolls, as in the present article). Alternatively, the DIW/rolling/sintering approach is applicable, without a decomposition step, to a variety of sinterable ceramics such as oxides (e.g., alumina and zirconia), resulting in ceramic scrolls. Finally, a displacement reaction is also possible: for example, titanium oxide scrolls were created by carrying out sintering of TiH_2 scrolls in air to oxidize the structure yielding TiO_2.[26]

Conclusions

A new approach to creating microarchitectured, reticulated titanium is demonstrated that consists of direct-write

assembly of a planar mesh, followed by rolling of the mesh into a scroll and sintering. The use of fine titanium powders (0.1 μm in size) in the ink results in good sintering, but high hardness indicative of high oxygen contamination and embrittlement. The use of coarser TiH$_2$ powders (22 and 65 μm in size) in the ink, which decompose to titanium during sintering, minimizes oxygen contamination in the scrolls as demonstrated by hardness values indicative of 0.55 wt% O. Two scrolls created with the 65 μm TiH$_2$ ink show a compressive stress–strain curve typical of ductile cellular metal, with extensive ductile compression eventually leading to densification. The observed stiffness and strength are in general agreement with a simple model assuming that filaments parallel to the applied stress are load-bearing in pure compression.

[1] M. Geetha, A. K. Singh, R. Asokamani, A. K. Gogia, *Prog. Mater. Sci.* **2009**, *54*, 397.

[2] G. H. van Lenthe, M. M. M. Willems, N. Verdonschot, M. C. D. Malefijt, R. Huiskes, *Acta Orthop. Scand.* **2002**, *73*, 630.

[3] H. Li, S. M. Oppenheimer, S. I. Stupp, D. C. Dunand, L. C. Brinson, *Mater. Trans, JIM* **2004**, *45*, 1124.

[4] V. Karageorgiou, D. Kaplan, *Biomaterials* **2005**, *26*, 5474.

[5] D. C. Dunand, *Adv. Eng. Mater.* **2004**, *6*, 369.

[6] R. Singh, P. D. Lee, R. J. Dashwood, T. C. Lindley, *Mater. Technol.* **2010**, *25*, 127.

[7] G. Ryan, A. Pandit, D. P. Apatsidis, *Biomaterials* **2006**, *27*, 2651.

[8] I. H. Oh, N. Nomura, N. Masahashi, S. Hanada, *Scr. Mater.* **2003**, *49*, 1197.

[9] M. Thieme, K. P. Wieters, F. Bergner, D. Scharnweber, H. Worch, J. Ndop, T. J. Kim, W. Grill, *J. Mater. Sci. Mater. Med.* **2001**, *12*, 225.

[10] B. Ye, D. C. Dunand, *Mater. Sci. Eng, A* **2010**, *528*, 691.

[11] M. Bram, C. Stiller, H. P. Buchkremer, D. Stover, H. Baur, *Adv. Eng. Mater.* **2000**, *2*, 196.

[12] Z. Esen, S. Bor, *Scr. Mater.* **2007**, *56*, 341.

[13] C. E. Wen, Y. Yamada, K. Shimojima, Y. Chino, T. Asahina, M. Mabuchi, *J. Mater. Sci. Mater. Med.* **2002**, *13*, 397.

[14] N. G. D. Murray, D. C. Dunand, *Compos. Sci. Technol.* **2003**, *63*, 2311.

[15] R. Ricceri, P. Matteazzi, *Int. J. Powder Metall.* **2003**, *39*, 53.

[16] Z. X. Guo, C. S. Y. Jee, N. Ozguven, J. R. G. Evans, *Mater. Sci. Technol.* **2000**, *16*, 776.

[17] J. H. Lee, H. E. Kim, K. H. Shin, Y. H. Koh, *Mater. Lett.* **2010**, *64*, 2526.

[18] N. A. Fleck, V. S. Deshpande, M. F. Ashby, *Proc. R. Soc. A* **2010**, *466*, 2495.

[19] Q. Li, E. Y. Chen, D. R. Brice, D. C. Dunand, *Metall. Mater. Trans. A* **2008**, *39*, 441.

[20] Q. Li, E. Y. Chen, D. R. Brice, D. C. Dunand, *Adv. Eng. Mater.* **2008**, *10*, 939.

[21] P. Moongkhamklang, D. M. Elzey, H. N. G. Wadley, *Composites Part A* **2008**, *39*, 176.

[22] P. Heinl, A. Rottmair, C. Körner, R. F. Singer, *Adv. Eng. Mater.* **2007**, *9*, 360.

[23] V. K. Balla, S. Bose, A. Bandyopadhyay, *Philos. Mag.* **2010**, *90*, 3081.

[24] L. E. Murr, S. M. Gaytan, F. Medina, H. Lopez, E. Martinez, B. I. Machado, D. H. Hernandez, L. Martinez, M. I. Lopez, R. B. Wicker, J. Bracke, *Philos. Trans. R. Soc. A* **2010**, *368*, 1999.

[25] D. A. Hollander, M. von Walter, T. Wirtz, R. Sellei, B. Schmidt-Rohlfing, O. Paar, H. J. Erli, *Biomaterials* **2006**, *27*, 955.

[26] B. Y. Ahn, D. Shoji, C. J. Hansen, E. Hong, D. C. Dunand, J. A. Lewis, *Adv. Mater.* **2010**, *22*, 2251.

[27] K. A. Erk, D. C. Dunand, K. R. Shull, *Acta Mater.* **2008**, *56*, 5147.

[28] J. E. Smay, J. Cesarano, J. A. Lewis, *Langmuir* **2002**, *18*, 5429.

[29] C. San Marchi, M. Kouzeli, R. Rao, J. A. Lewis, D. C. Dunand, *Scr. Mater.* **2003**, *49*, 861.

[30] M. V. Oliveira, R. P. Pereira, L. C. Pereira, *CBECIMat* **2008**, 5777.

[31] M. J. Donachie, *Titanium – A Technical Guide*, ASM, Metals Park, OH **1988**.

[32] D. J. Jorgensen, D. C. Dunand, *Acta Mater.* **2011**, *59*, 640.

[33] N. Tuncer, G. Arslan, *J. Mater. Sci.* **2009**, *44*, 1477.

[34] L. J. Gibson, M. F. Ashby, *Cellular Solids: Structures and Properties*, Cambridge University Press, NY **1997**.

[35] C. Zou, E. Zhang, M. Li, S. Zeng, *J. Mater. Sci. Mater. Med.* **2008**, *19*, 401.

[36] N. G. Davis, J. Teisen, C. Schuh, D. C. Dunand, *J. Mater. Res.* **2001**, *16*, 1508.

[37] L. P. Lefebvre, A. Blouin, S. M. Rochon, M. N. Bureau, *Adv. Eng. Mater.* **2006**, *8*, 841.

[38] D. T. Queheillalt, H. N. G. Wadley, *Acta Mater.* **2005**, *53*, 303.